# Solution-processed semiconductors for next-generation photodetectors

*F. Pelayo García de Arquer[1]*, Ardalan Armin[2]*, Paul Meredith[2,3] and Edward H. Sargent[1]*

Abstract | Efficient light detection is central to modern science and technology. Current photodetectors mainly use photodiodes based on crystalline inorganic elemental semiconductors, such as silicon, or compounds such as III–V semiconductors. Photodetectors made of solution-processed semiconductors — which include organic materials, metal-halide perovskites and quantum dots — have recently emerged as candidates for next-generation light sensing. They combine ease of processing, tailorable optoelectronic properties, facile integration with complementary metal–oxide–semiconductors, compatibility with flexible substrates and good performance. Here, we review the recent advances and the open challenges in the field of solution-processed photodetectors, examining the topic from both the materials and the device perspective and highlighting the potential of the synergistic combination of materials and device engineering. We explore hybrid phototransistors and their potential to overcome trade-offs in noise, gain and speed, as well as the rapid advances in metal-halide perovskite photodiodes and their recent application in narrowband filterless photodetection.

Photodetection underpins medical X-ray imaging, the ubiquitous visible light cameras, and emerging applications such as near-infrared medical imaging and short-wave infrared surveillance and machine vision. Present-day photodetection relies primarily on semiconductors that, depending on their bandgap, are able to transduce photons of different energies into electrical signals for subsequent processing, image reconstruction and storage. Historically, this has been enabled by the use of photodiodes and phototransistors made from crystalline inorganic semiconductors such as silicon or III–V compounds — materials heavily used in modern electronics and optoelectronics. Lithographically patterned arrays of photodiodes and phototransistors enable image sensors — arrays of miniaturized photodetectors — when combined with backplane architectures such as complementary metal–oxide–semiconductors (CMOS). Based on these materials, sensitive and fast image sensors have been developed, and this technology is now widespread in consumer electronics, mobile devices, vehicular systems, military applications and security. However, rapidly advancing applications such as self-driving cars, authentication systems, augmented and virtual reality, and point-of-need healthcare create an ever-increasing demand for innovations in imaging technology.

The miniaturized integration of inorganic semiconductor photoactive materials with read-out integrated circuitry (ROIC) complicates the design of devices and poses significant limits on the achievable compactness and sensitivity[1]. Commercially available image sensors rely on photodetectors combined with the ROIC through front-side or back-side integration, depending on the position of the active layer in the sensor stack. Conventional inorganic semiconductors are broadband absorbers; thus, they produce a broad spectral photoresponse. This creates the need to use input-side colour filter arrays and/or wavelength cutoff filters for colour imaging and colour-selective sensing, complicating the architecture and fabrication of devices and negatively affecting pure colour replication.

Low-temperature solution-processed semiconductors are an emerging class of photoactive materials that can be processed in ink form through wet chemistry. They are technologically attractive for several reasons: they can be deposited from solution over large areas using readily available manufacturing techniques, such as spin coating, roll-to-roll printing, spray coating and doctor blading (FIG. 1a), they are processed at low temperatures and under ambient conditions, and they are compatible with multiple ancillary material types (which can be used, for example, for contacts and transport layers), including flexible substrates (FIG. 1b). Their processing versatility is particularly advantageous for top-surface photodetection schemes. This approach allows for the direct incorporation of an ultrathin photoactive layer on top of the ROIC with high or even-unity fill factors (the photoactive fraction of the pixel area) and delivers compact, sensitive, high-resolution imaging systems (FIG. 1c). This is

[1]*Department of Electrical and Computer Engineering, University of Toronto, 35 St George Street, Toronto, Ontario M5S 1A4, Canada.*
[2]*School of Mathematics and Physics, The University of Queensland, St Lucia Campus, Brisbane 4072, Australia.*
[3]*Department of Physics, Swansea University, Singleton Park, Swansea SA2 8PP, Wales, UK.*

**These authors contributed equally to this work.*
*Correspondence to E.H.S.*
*ted.sargent@utoronto.ca*

doi:10.1038/natrevmats.2016.100
Published online 24 Jan 2017

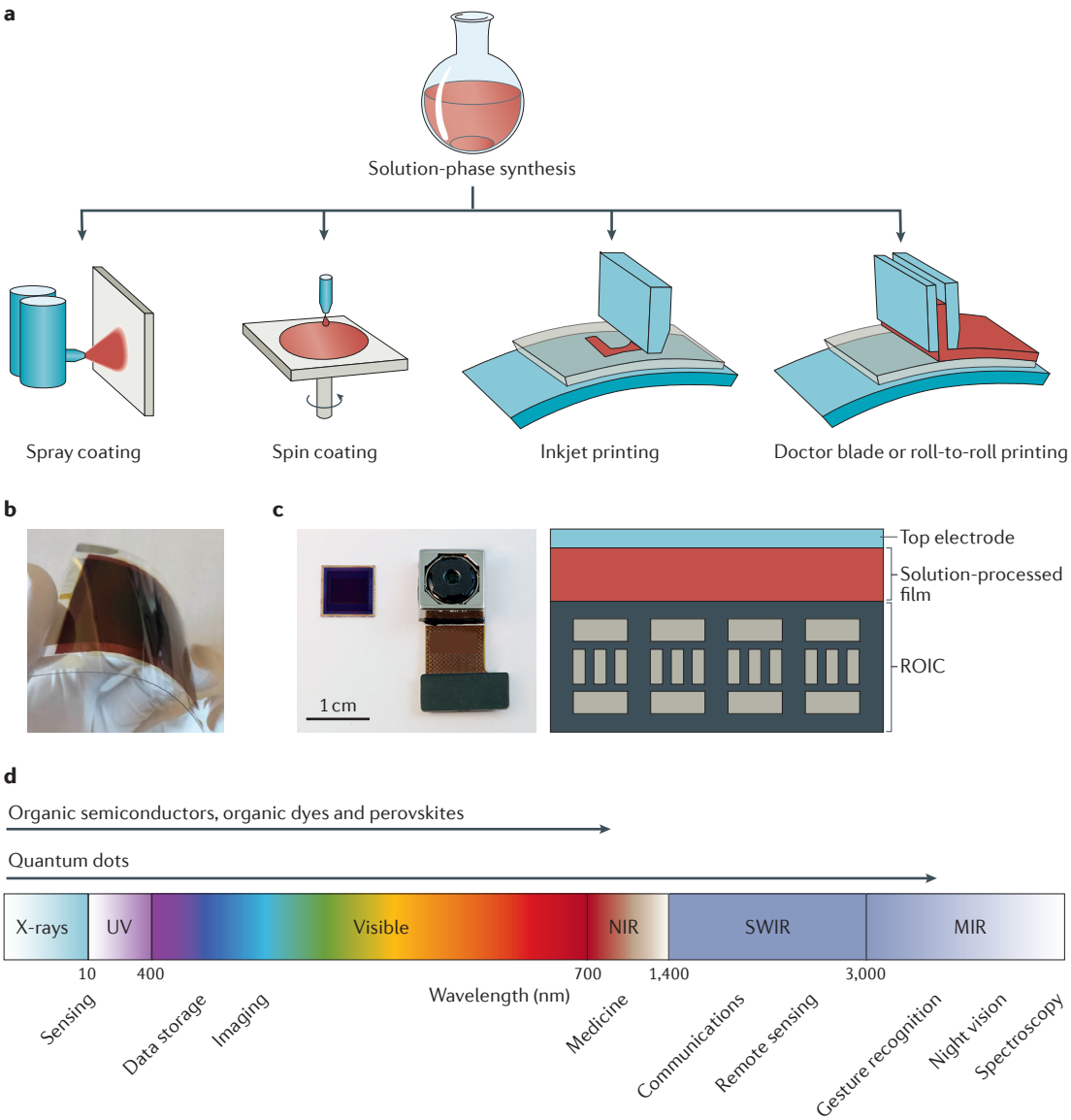


Figure 1 | **Solution-processed photodetectors. a** | Solution-processed materials are synthesized in the form of colloidal semiconductor inks. These can be deposited and assembled in solid films using spray coating or spin coating, or manufacturing techniques such as inkjet printing, doctor blading or roll-to-roll printing. **b** | These materials and deposition methods are compatible with a variety of flexible and unconventional substrates, and they ensure compatibility with current sensing technologies such as complementary metal–oxide–semiconductors. **c** | This ease of integration has led to new photodetection schemes such as top-surface photodetectors, in which the photoactive material is formed on top of the read-out circuit with total coverage, resulting in improved sensitivity and minimized crosstalk. A chip and a module incorporating the chip are shown, together with a schematic drawing of a top-surface photodetector. **d** | Typical solution-processed materials comprise organic semiconductors and dyes, organohalide perovskites, inorganic nanocrystals and quantum dots. The wide spectral range afforded by these materials allows applications from the X-ray to the mid-infrared spectral region. MIR, mid-infrared; NIR, near-infrared; ROIC, read-out integrated circuitry; SWIR, short-wave infrared; UV, ultraviolet. Panel **b** is reproduced with permission from REF. 6, Wiley-VCH.

especially important in the context of efforts to overcome the interconnection bottleneck that arises when attempting to further miniaturize sensor arrays while continuing to improve resolution and sensitivity.

In addition to the manufacturing benefits offered by solution-processed semiconductors, they have the advantage that their optoelectronic properties can be tailored. Especially appealing for photodetection is the ability to control the semiconducting optical gap and the electronic energetics. Solution-processed semiconductors include organic materials, metal-halide perovskites (MHPs), and inorganic nanocrystals and quantum dots; each of these classes of materials possesses (to lesser or greater extents) optoelectronic tunability and can be used to address a certain spectral range (FIG. 1d). In organic semiconductors, the optical gap can be tuned by varying the molecular structure and/or by controlling the solid-state assembly (morphology). In combination, these strategies allow

spectral photodetection coverage from the ultraviolet to the near-infrared. MHPs, on the other hand, are hybrid organic–inorganic compounds with the basic perovskite unit-cell structure, as their name suggests, and they are a more recent addition to the solution-processable semiconductor family. Compositional tuning of the organic and inorganic fractions allows the modification of the semiconductor bandgap from the visible through to the near-infrared. By contrast, quantum confinement in colloidal quantum dots (CQDs) enables tuning of their spectral response well into the infrared merely by adjusting the size of the nanocrystals during synthesis. Moreover, the band structure and the electronic energy levels of the resulting photoactive materials can be tailored by surface chemical engineering.

Advances in controlling and understanding these materials science aspects have led to state-of-the-art performance in a selected number of applications, and even to commercial deployment. Organic semiconductors display an almost limitless molecular diversity and show considerable potential for achieving colour discrimination through molecular[2] and device architecture[3] tuning, or through both strategies in combination[4]. Low-noise and broadband visible near-infrared light detection have been reported[5,6]. Inorganic CQDs with broader responses, up to the short-wave infrared, have been demonstrated[7–9]. These ultrasensitive photodetectors exhibit either strong intrinsic gain or fast photoresponse, and can be further improved by combining these two features. MHPs possess advantageous properties, such as large absorption coefficients, low exciton binding energy and high charge-carrier mobility, as a consequence of the combination of their organic and inorganic components[10,11]. Their rare collection of desirable properties makes them potentially suitable for photodetector applications.

Despite considerable recent progress in using solution-processed semiconductors for photodetection, several challenges and opportunities remain, both from a basic science and a device engineering perspective. Materials properties such as tunability can be used in new device architectures to implement additional functions such as multispectral sensing. Solution processing can be used to devise new materials, materials combinations and structures to overcome classic photodetection limitations, for example those associated with dark noise. It is also interesting to consider how conventional and new materials can be combined to create hybrid photodetectors with unrivalled performance.

This Review covers recent advances, ongoing progress and challenges in the field of solution-processed photodetectors from the perspective of both materials and devices. We begin by offering a broad overview of the past decade of advances. We particularly address the potential of MHP photodiodes — a hot topic in optoelectronics. We discuss how hybrid phototransistor architectures allow the overcoming of the conventional photodetection limits by decoupling noise, gain and speed. Finally, we cover the latest progress in narrowband filterless multispectral photodetection, and survey the new exciting avenues enabled by the synergistic combination of materials and device platforms.

## Photodetector architectures

Semiconductor-based photodetectors can be categorized into photoconductors, photodiodes and phototransistors[12]. In photoconductors, one type of charge carrier is recirculated through symmetrical contacts before it recombines with the opposite charge. An external voltage is applied to read out the photon-derived changes in conductivity, and gain can be achieved through multiple carrier recirculation. By contrast, photodiodes rely on the presence of a built-in potential in a junction to assist the extraction of the photogenerated carriers. Often, an additional reverse bias is applied to increase the charge collection efficiency. Phototransistors are optoelectronic amplifying switches in which a gate-programmable semiconducting channel can be optoelectronically modulated, aiding or hindering charge transport while simultaneously providing gain.

The performance metrics (BOX 1; TABLE 1) of relevant photodetectors based on different materials and architectures are summarized in TABLE 2.

***Organic semiconductor photodetectors.*** Electrical conductivity was discovered in doped polypyrrole[13] in the 1960s. During the 1970s and 1980s, myriads of small-molecule and polymeric conductors and semiconductors were synthesized, culminating in the demonstration of multiple optoelectronic device platforms including organic solar cells[14], field-effect transistors[15] and ultimately photodetectors[16].

The potential for organic photodetectors (OPDs) to achieve filterless narrowband colour sensing was recognized early, in the first homojunctions and linear heterojunctions[17]. However, these devices were limited by the excitonic nature of the organic semiconductors, which typically exhibit exciton binding energies of hundreds of millielectronvolts, severely affecting charge generation and hence transport and external quantum efficiency (EQE). This problem has been largely resolved by using bulk heterojunctions (BHJs), which are blends of two organic semiconductors (a donor and an acceptor) with different chemical potential energies, to aid charge separation. Efficient BHJ systems can exhibit EQEs in excess of 80% even at short circuit; thus most OPDs are based on BHJ photoactive layers in a diode architecture. Unfortunately, using two mixed components in the photoactive layer complicates the spectral response, because both the donor and the acceptor contribute to photogeneration[18]. Additional optoelectronic strategies must be used to produce a narrowband response in OPDs; we will return to this point later in the Review.

When evaluating the performance of OPDs, it is important to appreciate that organic semiconductors are electrically disordered. This leads to relatively low carrier mobilities for both carrier types, which in turn hinders photogenerated carrier collection and limits its performance metrics such as EQE, linear dynamic range and temporal response. Low carrier mobilities also constrain the junction thickness to typically <200 nm, meaning higher leakage currents and hence dark noise, and limiting the amount of light that can be absorbed in these thin films.

Organic semiconductors with improved packing and stronger intermolecular interactions have been synthesized and exhibit high hole mobilities, on the order of $10^{-2}$ $cm^2 V^{-1} s^{-1}$ in diodes. However, charge collection is still limited by the electron mobility of fullerenes ($\sim 10^{-3}$ $cm^2 V^{-1} s^{-1}$), which remain the predominantly used acceptor. Materials with improved transport properties should also allow for thicker junctions, reducing leakage and dark noise.

The optical gap of organic semiconductors can be tuned by modulating their conjugation length. Using this approach, broadband OPDs have been reported for various spectral bands, from the ultraviolet to the near-infrared. Visible-blind OPDs with high responsivity in the ultraviolet, linear dynamic range larger than 10 orders of magnitude and large gain have been reported[19]. Infrared-blind broadband visible OPDs have also been demonstrated using small molecules[20] and polymeric[21] semiconductors. In addition, it has been shown that optically thick polymer–fullerene BHJs made of PCDTBT:PC70BM can deliver an infrared-blind and spectrally flat photoresponse across the visible spectrum, with specific detectivity $D^*$ approaching $10^{13}$ Jones on large and flexible substrates[6] (for clarity, we will use Jones instead of cm $Hz^{1/2}$ $W^{-1}$ throughout the manuscript). This has been also demonstrated in fully printed PCDTBT:PC70BM photodiodes[22].

Progress in organic photodetectors is strongly coupled to improvements in organic solar cells, in particular to the use of new materials with narrower optical gaps[23,24] and to advances in the ability to manipulate the electro-optical properties of the devices[25,26]. Spectral responses up to 1,000 nm have been reported[20,21,27], but decreasing the optical gap of organic semiconductors to below 1 eV is challenging. An extension of the spectral response of broadband OPDs to 1,450 nm was obtained by using the narrow-gap polymer poly(5,7-bis(4-decanyl-2-thienyl)-thieno(3,4-b)diathiazole-thiophene-2,5), PTTT, blended with fullerene derivative PC60BM[5]. However, the mechanism by which a photoresponse can be generated past the donor gap is still to be elucidated.

A different approach has been used to extend the spectral bandwidth of photodetectors based on P3HT:PCBM blends, which are typically sensitive only to visible light. The introduction of PbS nanoparticles allowed spectral responses beyond 1,100 nm — an indication of charge and energy transfer from the nanoparticles to the polymer matrix — in a photodiode array prototype integrated into a ROIC panel[28]. The incorporation of ZnO nanoparticles was reported by different groups to result in photoconductive gain[19,29,30]. The addition of ZnO nanoparticles in P3HT:PCBM:PbS ternary blends was shown to deliver large EQEs (~1,000%)[30]. Hence, broadband OPDs with respectable performance metrics covering the ultraviolet to near-infrared range have been realized.

***Colloidal quantum-dot photodetectors.*** The bandgap tunability of CQDs from the visible to the infrared region has long been appreciated as a means to extend the range of OPDs. Preliminary efforts used CQDs as sensitizing agents in polymeric charge-transporting matrices[31]. Photophysical studies revealed that visible-light excitons in CdS could be transferred to the host matrix, giving rise to photoconductivity. CdSe visible photodetectors with an inferred $D^*$ of $10^8$ Jones (REF. 32) and short-wave infrared PbS CQD photodetectors were subsequently reported[33].

A new paradigm in solution-processed photodetection was demonstrated in 2006, when the sequential, ordered processing of PbS CQDs led to photoconductive CQD solid films[7]. The controllable fusing and oxidation of the CQDs delivered high photo-multiplicative gain as a consequence of minority carrier trapping, yielding gains in excess of 1,000, responsivities of ~2,700 A $W^{-1}$ and impressive measured $D^*$ of up to $2 \times 10^{13}$ Jones in the short-wave infrared. This milestone sensitivity is higher than that of epitaxially deposited InGaAs photodetectors

Box 1 | **Performance metrics for photodetectors**

Photodetector performance is conventionally measured in terms of several different metrics that are associated with efficiency, noise and speed (TABLE 1). A basic, standalone figure of merit that quantifies the strength of the photoresponse is the responsivity ($R$), which relates the generated photocurrent (or photovoltage) to a given incident power. Gain ($G$) exists when the number of extracted photocarriers per absorbed photon exceeds unity. The temporal response of a photodetector is typically characterized by its −3dB bandwidth (the modulation frequency at which the photoresponse is half of that obtained under continuous illumination). This quantity depends on the carrier transit time ($t_{tr}$) and on the $RC$-time of the circuit:

$$f_{-3dB}^2 = \left(\frac{3.5}{2\pi t_{tr}}\right)^2 + \left(\frac{1}{2\pi RC}\right)^2 \quad (1)$$

In dispersive materials, such as organic semiconductors, the relevant transit time defining the frequency response is the slower carrier's transit time[6].

Another important quantity is the linear dynamic range (LDR), which measures the range of incident light irradiances ($L_{min}$ to $L_{max}$) over which the photoresponse is linear. In image sensors, this figure of merit conveys the range incident of optical powers over which images can be captured with high fidelity. This can be expressed in terms of number of decades or logarithmically (in dB); to quantify the LDR in dB, both $LDR = 20 \times \log(L_{max}/L_{min})$ and $LDR = 10 \times \log(L_{max}/L_{min})$ are used. The latter is used when the linearity of the power as a function of voltage is under question. A careful comparison between the LDRs of different devices needs to be carried out to avoid confusion between different logarithmic factors[5]. Special care must be taken when estimating the LDR from log–log plots, because this procedure can potentially result in its overestimation[5,63,106–109].

Ultimately, the sensitivity of a photodetector is determined by its ability to deliver a signal-to-noise ratio (SNR) that is high enough with respect to the noise current ($I_N$). The noise-equivalent power (NEP) represents the incident power that would be required to yield a near-unity SNR over a bandwidth of 1 Hz.

The overall figure of merit for photodetection, which normalizes the NEP to the device area ($A$) and electrical bandwidth of the noise measurement ($B$), is the specific detectivity ($D^*$). $D^*$ corresponds to the SNR if the detection bandwidth is 1 Hz and the device area is 1 $cm^2$ at an incident power of 1 W, and can be written as:

$$D^* = \frac{R\sqrt{AB}}{I_N} \quad (2)$$

Many sources can contribute to the noise current, including thermal, shot, flicker ($1/f$) and generation–recombination noise[93,110]. We note that the noise current cannot be directly inferred from the shot noise (simply defined by the dark current) and thermal noise in disordered semiconducting systems. In organic semiconductors, metal-halide perovskites and colloidal quantum-dot photodetectors, the actual measured noise can often exceed the root mean square of shot and thermal noises. Thus, inferring $D^*$ from a dark-derived theoretical estimate of shot noise can result in its overestimation.

Table 1 | **Photodetector metrics of performance**

| Metric | Unit | Definition |
|---|---|---|
| Photocurrent ($I_{ph}$) | A | Current flowing through a device owing to illumination |
| Dark current ($I_d$) | A | Current flowing in the absence of illumination |
| Responsivity ($R$) | A $W^{-1}$ (V $W^{-1}$) | Ratio of the photocurrent/photovoltage to the incident optical power |
| External quantum efficiency (EQE) | % | Number of carriers circulating divided by the number of incident photons |
| Gain ($G$) | Unitless | Number of collected carriers divided by the number of photons absorbed |
| −3dB bandwidth (BW) | Hz | Modulation frequency at which the responsivity of the device is half of that at steady state conditions |
| Linear dynamic range (LDR) | dB | Range of incident optical powers for which the detector responds linearly |
| Noise current ($I_N$) | A $Hz^{-1/2}$ | Root mean square of current fluctuation |
| Noise-equivalent power (NEP) | W $Hz^{-1/2}$ | Optical power that would be required to generate the given noise current spectral density $I_N/B^{1/2}$. It is a measure of the sensitivity of the device (NEP = $(I_N/B^{1/2})/R$) |
| Specific detectivity ($D^*$) | cm $Hz^{1/2}$ $W^{-1}$ (Jones) | NEP normalized to the area of the device ($A$) and to the electrical bandwidth of the noise measurement ($B$): $D^* = A^{1/2}/\text{NEP} = R(AB)^{1/2}/I_N$ |
| Spectral selectivity (FWHM) | nm | Full width at half maximum resonance width |

and offers the manufacturing benefits associated with solution-processed materials. The high photoconductive gain also opens new avenues for integrated in-pixel amplification, greatly simplifying sensor design. Visible photoconductors that make use of CQD bandgap tunability were also reported[34].

The controlled introduction of defects led to high gain and detectivity, but at the expense of a sub-20-Hz temporal response. The identification of the associated trap states and of surface chemistry strategies enabling their selective passivation led to improvements in the response times (down to below ~25 ms), but also resulted in reduced gain. Although sufficient for most imaging applications, this gain–bandwidth product limitation represents a marked drawback for higher-speed applications, such as in-flight object recognition[35,36]. Further improvements in CQD films that addressed their most acute limitation — the mobility — led to the realization of films with faster photoconductive responses (0.4 kHz bandwidth), with high internal gain ($G > 6.5 \times 10^3$) and detectivity ($D^* \approx 10^{13}$ Jones)[37].

The generation of multiple carriers per incident photon in CQDs can be achieved through multiple exciton generation. This process relies on the generation of multiple excitons when the energy of the incoming photon is several times greater than the semiconductor optical gap. The potential of this process has been explored in several material systems and architectures[38–42].

The successful implementation of CQD solids into full photodiode architectures remained elusive until 2007, partly owing to a limited understanding and control of the energy levels, surface chemistry and density of defect states[43]. Record sensitivity–bandwidth combinations, with $D^*$ exceeding $10^{12}$ Jones in the short-wave infrared and a −3dB bandwidth up to 5 MHz, were achieved in Schottky PbS CQDs photodiodes; this was accomplished by a combination of improved carrier mobility due to a more complete ligand exchange and a carrier extraction strategy that ensured that drift collection dominated over diffusion[8]. Heterojunction architectures with p–n geometry based on wide-bandgap metal oxides[44], polymers[28] and fullerene derivatives[45] have also been reported to have high detectivities.

The CQD bandgap tunability can also be used to engineer graded energy landscapes designed to funnel photogenerated carriers with the aid of a graded electric field[46]. These quantum-funnel photodiodes benefit from improved drift-assisted carrier extraction, yielding megahertz −3dB bandwidths even at zero bias and high detectivity in the near-infrared.

The compromise between carrier extraction and absorption efficiency characterizing CQD films gave rise to attempts to integrate photonic and plasmonic systems with CQD films to reduce the electrical volume of the photoactive material without sacrificing absorption. This approach resulted both in reduced carrier transit times (thus in a faster photoresponse) and in lower dark currents and noise, ultimately leading to high sensitivities, as long as the volume reduction compensated for the increasing surface recombination and contact noise arising from the higher surface-to-volume ratio. Improvements in responsivity[47,48] and detectivity[49] have been pursued through the incorporation of metallic nanostructures into the photodetector architecture. Special care should be taken when integrating these metallic motifs within the CQDs, as they can remotely modify the electrical properties of the quantum dot solid film[50]. Indeed, metallic nanostructures can improve the photodetector properties through remote doping and passivation mechanisms[51].

***Metal-halide perovskite photodetectors.*** The advent of MHPs has led to a considerable step forward in photovoltaics and opened promising avenues for photodetection. Perovskites, in general, have a crystal unit cell of the type $ABX_3$, where B is a cation and X is an anion, forming an octahedron $[BX_6]^{4-}$ (FIG. 2a). The octahedra are stabilized by a second cation A; a simple and archetypal example of this structure is $CaTiO_3$. In organohalide lead perovskites, the cation A is a small organic molecule, such as methylammonium ($CH_3NH_3^+$) or formamidinium ($H_2NCHNH_2^+$), B is a metal such as lead or tin, and X is a halide combination. The use of MHPs in optoelectronics is compelling: they can be solution-processed from simple Earth-abundant precursors[11] or evaporated using relatively low deposition temperatures in a similar way to organic semiconductors; they have energy bandgaps that are tunable with the halide ratio; and they can form efficient thin single photojunctions using simple planar or mesoporous scaffold-based architectures owing to their low exciton binding energy[52], similar to that of inorganic semiconductors. As such, MHPs combine the advantages of inorganic and organic semiconductors. The non-excitonic behaviour of optimized MHP films results in the simplest possible diode architecture, in which charges can be photogenerated and collected almost without loss (FIG. 2a,b).

More than 2 years after the demonstration of the first efficient MHP solar cells[53,54], $CH_3NH_3PbI_3$ was used in photoconductors in 2014 (REF. 55) and the first low-noise MHP photodiodes were reported in 2015 almost simultaneously by four research groups[56–59]. The reason behind this relatively long delay is that MHPs were initially deployed in metal oxide mesoporous scaffolds, which are not suitable for photodetection owing to their large capacitances. Planar junctions became more common[60] in 2014; however, solution processing of these junctions was not trivial. Low-noise photodetection requires very high-quality and dense active layers to prevent leakage

Table 2 | **Figures of merit and progress of solution-processed photodetectors**

| Year | Spectral region | EQE/*R*/*G* | *D** (Jones) or NEP (measured) | *D** (Jones) (inferred)‡ | BW | LDR | Type | Material | Features | Refs |
|---|---|---|---|---|---|---|---|---|---|---|
| 1996 | Vis | 0.2 A W$^{-1}$ | – | – | – | – | PC | CQD (CdX) | Early CQD photodetector | 31 |
| 1998 | UV–Vis | 0.2 A W$^{-1}$ | – | – | – | – | PD | Polymer | Image sensor with colour filter | 114 |
| 2003 | Vis | 0.2 mA W$^{-1}$ | – | – | – | – | PD | Polymer | Colour selectivity using microcavity | 26 |
| 2004 | UV–green | 0.7 mA W$^{-1}$ | – | – | – | – | PT | Polymer | Solution-processed phototransistor | 115 |
| 2005 | Vis | EQE 15% | – | $10^8$ | 50 kHz | – | PC | CQDs (CdSe) | – | 32 |
| 2006 | Vis–1.6 μm | 2,700 A W$^{-1}$ | $2\times10^{13}$ | $7\times10^{12}$ | 20 Hz | – | PC | CQDs (PbS) | Pure CQDs: ultrasensitive and high gain | 7 |
| 2007 | Vis–NIR | 120 A W$^{-1}$ | $5\times10^{12}$ | $3\times10^{13}$ | 20 Hz | 150 dB | PT | CQDs (PbS) | Exploiting CQD tunability for visible photodetection | 34 |
| 2007 | NIR | 0.6 A W$^{-1}$ | NEP $1.35\times10^{-11}$ | – | 4 MHz | – | PD | Polymer | NIR response using polymers | 21 |
| 2008 | X-ray | 5 mA W$^{-1}$ | X-ray sensitivity 7 mGy s$^{-1}$ | – | – | – | PD | Polymer or fullerene | Low noise enabling X-ray detection | 116 |
| 2009 | Vis–NIR | 0.2 A W$^{-1}$ | – | $1\times10^{12}$ | – | 100 dB | PD | Polymer | NIR sensitivity | 5 |
| 2009 | Vis–NIR | $G\approx85$ | – | – | 30 | – | PC | CQDs (PbS) | Exploiting MEG | 39 |
| 2009 | Vis–1.6 μm | EQE 50% | $10^{12}$ | – | 5 MHz | – | PD | CQDs (PbS) | Ultrafast | 8 |
| 2011 | Vis | 2.5 A W$^{-1}$ | $10^{13}$ | – | 0.4 kHz | – | PC | CQDs (CdS or CsSe) | High mobility | 37 |
| 2012 | UV | 1,000 A W$^{-1}$ | $7\times10^{15}$ | – | 600 Hz | – | PD or PC | NCs (ZnO or MHP-PT) | Photodiode to photoconductor switch | 29 |
| 2012 | Vis–1.6 μm | $10^7$ A W$^{-1}$ $G=10^8$ | $7\times10^{13}$ | – | 30 Hz (gated) | – | PT | CQDs (PbS-g) | Hybrid phototransistor and ultrahigh gain | 69 |
| 2013 | UV–Vis | 0.2 A W$^{-1}$ | $4\times10^{11}$ | – | 20 kHz | 180 dB | PD | Fullerene | Large LDR | 117 |
| 2014 | Vis | 0.33 A W$^{-1}$ | $10^{13}$ | – | 200 kHz to 2 MHz | 180 dB | PD | Polymer | Large LDR, low noise, spectrally flat and large area | 6 |
| 2014 | Vis–1.6 μm | $6\times10^5$ A W$^{-1}$ | $5\times10^{11}$ | $10^{15}$ | 10 Hz | – | PT | CQD + $MoS_2$ | High gain combined with channel dark current suppression | 74 |
| 2014 | UV | 3 A W$^{-1}$ | – | – | 1.7 Hz | – | PC | MHP | Large area, flexible | 55 |
| 2014 | UV–Vis | 0.3 A W$^{-1}$ | – | $8\times10^{13}$ | 3 MHz | 100 dB | PD | MHP | High sensitivity | 57 |

current. A reliable and reproducible solution-processing method to produce planar MHP layers was introduced late in 2014, enabling planar junction diodes[61].

In the four seminal reports on MHP photodiodes, both inverted and conventional architectures were used, and PCBM and/or fullerene were used as electron-extracting and hole-blocking interlayers. In these reports, $D^* \approx 10^{12}$ Jones and EQEs of 60 to 80% in the visible region were achieved. The response speed in these photodiodes was shown to be *RC*-time limited[56] (meaning that the second term of equation 1 in BOX 1 is the dominant one), with a response time of 120 ns (REF. 59); this is predominantly because of the large dielectric constant of MHPs (70 to 30 from static to 1 MHz frequencies)[52]. The use of thick fullerene buffer layers can reduce the capacitance with no detrimental effect on the device performance and increase the −3dB response from 100 to 500 kHz. For small pixels, the response speed becomes limited by the carrier transit time and can exceed a megahertz in MHP photodiodes[56,57,59].

As with organic semiconductor photodiodes, the electro-optical properties of MHPs can be tuned by changing the composition of the perovskite material (FIG. 2c). Recently, $CH_3NH_3PbI_3$ active layers in which the ratio of $PbI_2/CH_3NH_3I$ was optimized in a trap-engineered diode architecture were used to obtain photoconductive gains up to 400 with a response speed of microseconds and 85 dB of linearity[62] (FIG. 2d). Similar to organic semiconductors, MHPs can also be combined with inorganic nanoparticles. The use of PbS quantum dots to expand the spectral bandwidth of MHPs to the NIR was recently reported[63], and a new strategy to modulate MHPs optical and electrical properties based on molecular doping was suggested[64].

MHPs also attracted attention for X-ray detection[65,66]. Owing to the large atomic number of lead, its compounds have large X-ray absorption coefficients; this led to the study of semiconducting lead halides as potential candidates for X-ray detectors[67]. These large absorption

Table 2 | **Figures of merit and progress of solution-processed photodetectors (cont.)**

| Year | Spectral region | EQE/*R*/*G* | *D** (Jones) or NEP (measured) | *D** (Jones) (inferred)‡ | BW | LDR | Type | Material | Features | Refs |
|---|---|---|---|---|---|---|---|---|---|---|
| 2015 | Vis–1.1 μm | EQE 80% | $2\times10^{13}$ | – | 1 MHz | – | PD | CQD (PbS) | Quantum funnel | 46 |
| 2015 | Vis–NIR | *G* = 10 | – | – | 35 kHz | – | PT | CQD (PbS) | Phototransistor, overcoming gain–dark current trade-off | 78 |
| 2015 | Red and NIR | 0.1 A W$^{-1}$ | $5\times10^{12}$ | – | 90 kHz | 160 dB | PD | Polymer | Colour selectivity, CCN | 3 |
| 2015 | Vis | 0.3 A W$^{-1}$ | $2\times10^{13}$ | – | 50 kHz | 100 dB | PD | Polymer | Fully printed | 22 |
| 2015 | NIR | 0.12 A W$^{-1}$ | – | $10^{12}$ | – | – | PD | Organic dye | Transparent, NIR sensitivity | 118 |
| 2015 | UV–Vis | 0.25 A W$^{-1}$ | $3\times10^{12}$ | – | 450 kHz | 230 dB | PD | MHP | Increased BW using buffer layer | 56 |
| 2015 | UV–Vis | 0.3 A W$^{-1}$ | $8\times10^{12}$ | – | – | 190 dB | PD | MHP | Low noise | 59 |
| 2015 | UV–Vis | 0.4 A W$^{-1}$ | $10^{12}$ | – | 290 kHz | 80 dB | PD | MHP | Low noise and stability | 58 |
| 2015 | UV–Vis | *G* ≈ 300 | NEP 0.18 pW | – | 8 kHz | 170 dB | PD | MHP | High gain through trap engineering | 62 |
| 2015 | X-ray | $2\times10^4$ carriers per photon | 25 mGy cm$^{-2}$ | – | 3 GHz | – | PD | MHP | X-ray sensor | 65 |
| 2015 | UV–Vis | 5 mA W$^{-1}$ | $2\times10^{10}$ | – | 600 Hz | – | PD | MHP | Narrowband response through CCN in single crystals | 104 |
| 2015 | UV–Vis | 0.1 A W$^{-1}$ | $2\times10^{11}$ | – | 0.3 MHz | 120 dB | PD | MHP | Narrowband response through doping, CCN | 64 |
| 2016 | X-ray | 16.4% | 80 μC Gy$^{-1}$ cm$^{-2}$ | – | 1.6 kHz | – | PC | MHP | High sensitivities above standard Se detectors enabled by MHP single-crystal properties | 67 |
| 2016 | UV–NIR | $3\times10^5$ A W$^{-1}$ | $2.5\times10^{12}$ | – | 100 Hz | – | PT | CQD + $MoS_2$ | Interface passivation in hybrid phototransistors | 80 |
| 2016 | UV–SWIR | EQE 70–80% | $4\times10^{12}$ | – | 1.5 kHz | 110 dB | PT or PD | CQD + graphene | Hybrid photodiode–phototransistor maximizes charge injection | 81 |
| 2016 | UV–NIR | $4\times10^9$ A W$^{-1}$ | $5\times10^{17}$ | – | 0.03 Hz, 35 kHz (gated) | – | PC | CdTe | Electrostatic trapping and percolation transport enables ultrasensitive photodetection | 87 |

‡It is important to note that in several published works, the specific detectivity (*D**) is inferred from the shot-noise ($S_N = (2qI_d)^{1/2}$, where $S_N$ is the noise spectral density, *q* is the charge and $I_d$ is the photocurrent), neglecting the thermal noise, which gives a non-trivial contribution. This can lead to a severe overestimation of *D**, especially in nanostructured photodetector systems that are dominated by flicker noise (1/*f*) at frequencies below 1–10 kHz. BW, −3dB bandwidth; CCN, charge collection narrowing; CQD, colloidal quantum dot; EQE, external quantum efficiency; *G*, gain; LDR, linear dynamic range; MEG, multiple exciton generation; MHP, metal-halide perovskite; NC, nanocrystal; NEP, noise-equivalent power; NIR, near-infrared; PC, photoconductor; PD, photodetector; PT, phototransistor; *R*, responsivity; SWIR, short-wave infrared; UV, ultraviolet; Vis, visible.

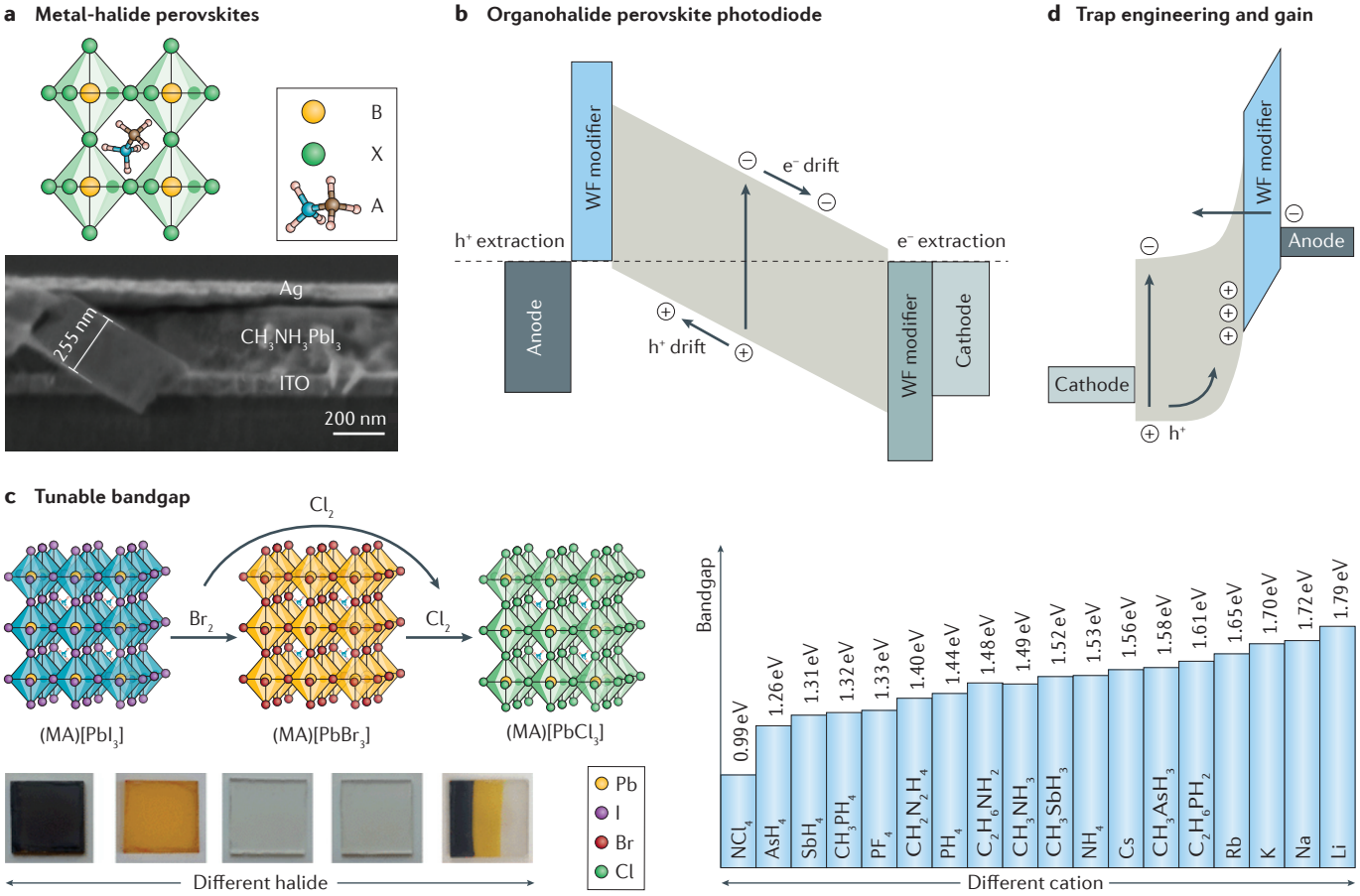


Figure 2 | **Metal-halide perovskite photodiodes. a** | Metal-halide perovskites are a class of hybrid organic–inorganic materials with a perovskite unit-cell structure (top). They consist of two cations (A and B) and an anion X that bonds them together. A cross-sectional scanning electron micrograph of a methylammonium lead trihalide perovskite photodiode is shown (bottom). **b** | Principle of operation of organohalide perovskite photodiodes. The collection of photogenerated carriers towards selective anode and cathode electrodes is drift-assisted. **c** | The bandgap of metal-halide perovskites can be widely tuned across the visible–near-infrared region by halide or cation modification[111,112]. In the left example, tunability is achieved by exposing the perovskite films to different halides (I, Br or Cl). The photographs show, left to right, $MAPbI_3$; $MAPbI_3$ exposed to $Br_2$; $MAPbCl_3$ obtained by exposing $MAPbI_3$ to both $Br_2$ and $Cl_2$ gases, or just to $Cl_2$; in the rightmost sample, only partial areas of the sample have been exposed. The choice of different cations allows the bandgap to be tuned from the visible to the short-wavelength infrared (right). **d** | Device and interface engineering can lead to functionalities typical of colloidal quantum-dot photodetectors, such as internal gain. ITO, indium tin oxide; WF, work function. Panel **a** is adapted with permission from REF. 113, Wiley-VCH. Panel **c** is adapted with permission from REF. 111, Royal Society of Chemistry and REF. 112, Macmillan Publishers Limited. Panel **d** is adapted with permission from REF. 62, Wiley-VCH.

coefficients, combined with the high mobilities and low defect density of organolead halide perovskites, led to the realization of fast and high-gain (over $10^4$ carriers per photon) X-ray photodetectors. One of the challenges encountered in this approach is the relatively large junction thickness (on the order of 1 mm) required to absorb a significant fraction of the X-ray photons impinging on the device. This demands long carrier diffusion lengths to avoid excessive recombination. Single-crystal methylammonium lead tribromide perovskite detectors with record mobility–lifetime products ($\sim 1 \times 10^{-2}\,cm^2\,V^{-1}$) and small surface charge recombination have recently been reported, showcasing sensitivities that exceed that of standard amorphous selenium detectors ($80\,\mu C\,Gy^{-1}\,cm^{-2}$)[66].

In summary, MHPs have emerged as materials with considerable potential for optoelectronics and especially photodetection. There are, however, many unanswered questions regarding their basic operational principles, such as their dielectric relaxation and ionic behaviour, and how these relate to photogeneration and collection.

In the next section, we examine how advances in device design, in particular the introduction of hybrid phototransistor architectures, can overcome traditional photodetection trade-offs in terms of noise, photoresponse and speed.

## Hybrid phototransistor architectures

In phototransistors, the electrical properties of a charge-transporting channel are modulated with light. There are several possible phototransistor architectures. Metal–oxide–semiconductor transistors are three-terminal devices that consist of a metallic gate (typically

Si), an oxide insulator (typically $SiO_2$) and a photoactive channel fabricated atop and contacted with drain and source electrodes. The advent of solution-processable materials enabled the introduction of thin-film phototransistors, which overcome the rigidity limitations of crystalline Si-based devices. Initially, thin-film phototransistors mainly relied on organic materials for the photoactive channel[16], which allowed their integration with flexible substrates[68]. Despite this advantageous property, the performance of these detectors has remained modest, largely owing to poor carrier mobilities in the photoactive channel.

Progress was reported in 2012 with the introduction of a hybrid combination of solution-processed and high-conductivity 2D materials[69]. In this type of device, photosensitization and transport take place in separately optimized phases, one enabling efficient light absorption and one providing fast charge recirculation. The combination of PbS CQDs and graphene resulted in ultrahigh gain ($G \approx 10^8$ electrons per photon) and exceptional responsivities for short-wave infrared photodetection. The CQD film was assembled and crossed-linked to the graphene transport layer with 1,2-ethanedithiol ligands, which aided charge injection into the graphene and provided electron trap states yielding a large photoconductive gain. The measured $D^* \approx 7 \times 10^{13}$ Jones represented a considerable step forward for visible–short-wave infrared imaging, yet the ~10 ms temporal response represented a serious limitation.

The enhanced performance of these hybrid devices stems from the separation of photosensitization (in the photoactive layer) and electrical transport (in the transport layer, FIG. 3a). If an appropriate gate bias $V_g$ is applied, the transport channel is closed in the dark. Under illumination, photogenerated charges separate owing to the internal electrical field existing at the gated junction, and one type of carrier (for example holes) is injected into the transport channel. This charge carrier can recirculate several times before a lower-mobility opposite carrier recirculates as well (or else becomes trapped). The photoconductive gain under such conditions is given by

$$G = \frac{t_{rec}}{t_{transit}} = \frac{t_{rec}}{L/v} \quad (1)$$

where $t_{rec}$ is the time required for the captured charge to be released and recombine in the sweeping electrodes, $L$ is the channel length and $v$ is the velocity of the injected charge. The excellent mobility of 2D semiconductors such as graphene (~$10^5$ $cm^2 V^{-1} s^{-1}$ at room temperature) therefore enables extraordinarily high photomultiplicative gains without limiting the temporal response of these devices, which is determined by the slowest process between charge injection and recombination.

In a similar manner, other groups reported the implementation of solution-processed materials combined with graphene in hybrid phototransistors. Large-area and flexible infrared detectors with excellent stability were fabricated[70] using PbS CQD solid films cast and assembled with pyridine ligands on top of chemically vapour-deposited graphene; these detectors achieved a responsivity of $R \approx 10^7$ A $W^{-1}$. MHP–graphene phototransistors, in which $CH_3NH_3PbBr_2I$ provided visible sensitization, have also been reported[71,72]. Pure MHP phototransistors based on $CH_3NH_3PbI_{3-x}Cl_x$ perovskites have also been explored and exhibited bipolar behaviour with response times of less than 10 µs in operation but gains below $10^3$ (REF. 73).

However, the absence of a bandgap in graphene precludes the full exploitation of this hybrid architecture because the transport channel cannot be totally closed, which ultimately results in considerable dark currents. Hence, the use of other high-mobility gapped materials is being explored, and the emergence of 2D materials with exceptional transport properties and bandgaps in the visible region, such as $MoS_2$, has spurred further development in the field. Hybrid phototransistors made of PbS CQDs and $MoS_2$ that benefited from significantly lower dark currents (over an order of magnitude) while maintaining high responsivities were reported[74]. The introduction of interface states as a consequence of the chemical modification of the transport layer deteriorates the noise and time response characteristics, and improvements can be expected provided these issues can be solved[75,76].

Other hybrid phototransistor architectures based on the combination of ZnO nanocrystals, PbS CQDs and organic semiconductors with ultraviolet–infrared photon-counting capabilities were also reported[77].

The separation of transport and sensitization can be also achieved in simpler architectures. Photojunction field-effect transistors rely on the presence of a high-resistance depletion region between a pair of source and drain non-ohmic contacts (FIG. 3b). Under dark conditions, this ensures that the noise level is minimal. When the device is illuminated, photogenerated charges split owing to the junction-gate effect, and the two types of carriers accumulate at the opposite sides of the material. The accumulation of one type of photogenerated carrier between the source and drain leads to a shift of the Fermi level which, if the system is adequately designed, aligns with the work functions of the electrodes, aiding charge collection when a voltage is applied. This was first implemented by using a softly n-doped PbS CQD layer depleted by a $MoO_3$ layer with a deep work function[78]; this architecture provides gain and at the same time overcomes the response/speed/dark-current trade-off that normally characterizes photoconductors. This is achieved by ensuring that, under dark conditions, the channel is fully depleted owing to the presence of a rectifying junction between the deep-work-function material and the CQD layer. A rise time of 10 µs was achieved in a gain-providing device, with an improvement in the photocurrent-to-dark-current ratio of two orders of magnitude compared to photoconductors.

In summary, the use of solution-processable materials allows the realization of hybrid phototransistor architectures with the potential to overcome traditional photodetection limitations posed by the dark current/gain/temporal response trade-off. In the next section, we discuss how solution-processable semiconductor photodetectors compare with incumbent technologies and explore the innovations that they provide.

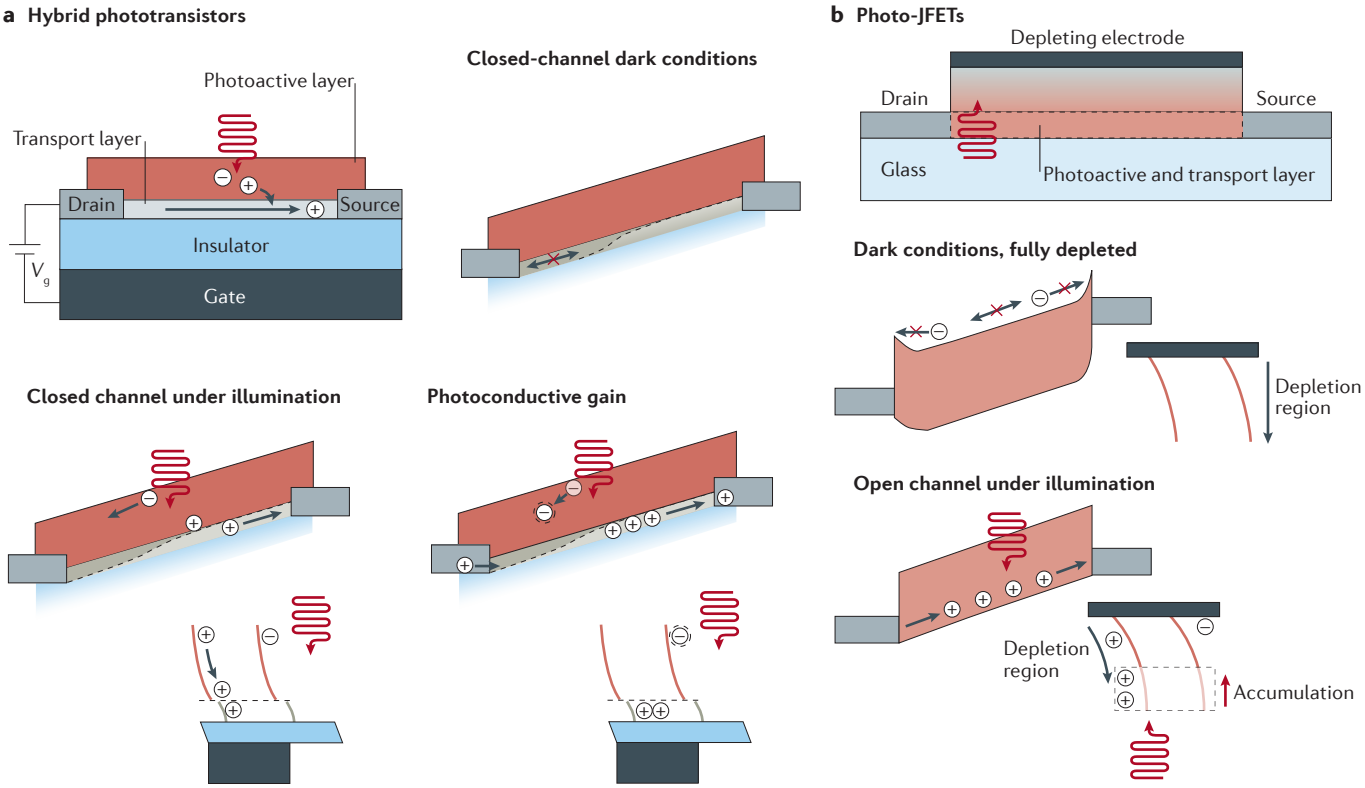


Figure 3 | **Phototransistors, gain and transport. a** | A schematic representation is shown of the operation of hybrid phototransistors separating electrical transport and optical sensitization. A transport channel is modulated by an external gate voltage ($V_g$) and ideally closed under dark conditions. Under illumination, charges are generated in the photoactive material. Depending on the gate voltage, one type of carrier (holes in this case) is injected into the transporting medium, whereas the opposite type of carrier remains in the photoactive material. Given appropriate and favourable transport properties, injected charges can recirculate several times before recombination, thus producing gain under illumination. **b** | In photojunction field-effect transistors (photo-JFETs), a channel is formed under illumination, because the otherwise depleted material does not favour circulation between the source and drain Schottky back-to-back electrodes. The use of this architecture provides gain while overcoming the response/speed/dark-current trade-off that normally characterizes photoconductors.

## Challenges and new approaches

In terms of detectivity, solution-processed semiconductor-based photodetectors can now compete with standard elemental inorganic crystalline semiconductors (such as Si or Ge) and high-temperature epitaxial semiconductor (such as InGaAs or HgCdTe) photodetectors (FIG. 4a). Now that this relevant metric of performance is on a par with these established technologies, the incorporation of solution-processed photodetectors with read-out integrated circuits is of great interest. The management of the interface between the different materials will play a crucial role in achieving efficient charge transfer from each pixel[79]. The compatibility of the chemical processing with the metal electrodes must be ensured, and this is especially important for halide-containing materials such as MHPs. The stability of the devices under operating conditions can be further improved to meet ever more demanding application requirements. Inter-pixel reproducibility is also an important factor that needs to be considered in material systems in which grain sizes are comparable with the pixel area (such as MHPs).

From the point of view of performance, marked improvements can be expected from the hybrid phototransistor architecture owing to the breaking of the gain–dark-current compromise. Prominent advances could be made by maintaining, or even increasing, the modulation of the transport channel, which is often altered upon incorporation of the photoactive layers. The control of the interface and of the contacts is expected to have an important role in this architecture's near future. The reduction of the number of interfacial trap states is important to achieve high subthreshold swings (the amount of voltage required to produce a one-decade change in the dark current) that increases the signal-to-noise ratio[80]. The growing number of available 2D materials, combined with the improved understanding of the optoelectronic properties of the photosensitizing layer, indicates a promising future for this device architecture.

Charge management within the photosensitizing layer is expected to result in greater control over carrier injection into the transport phase. This has recently been explored by incorporating a photodiode in the device to

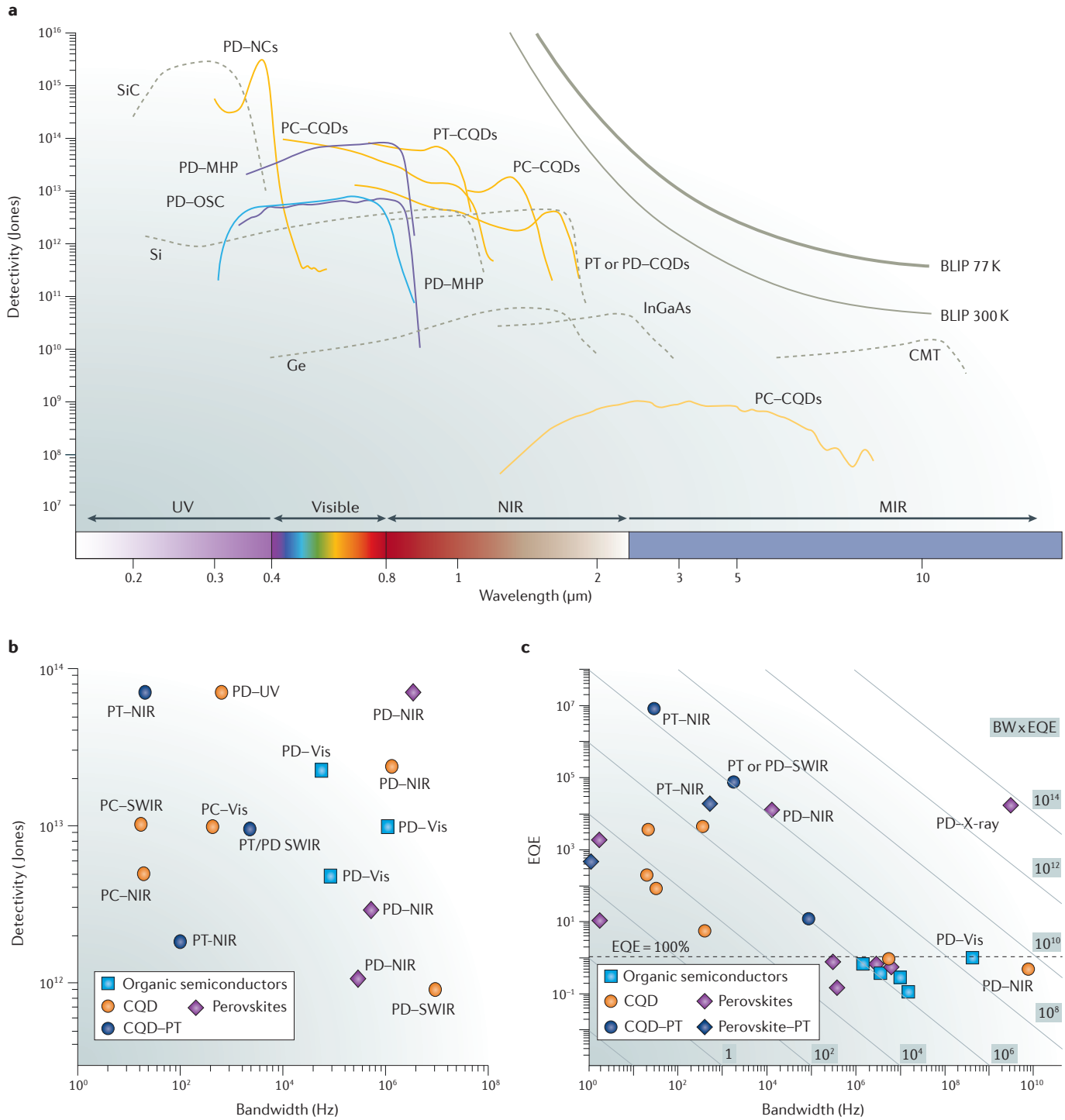


Figure 4 | **Performance metrics for solution-processed photodetectors. a** | Specific detectivities are shown for the best solution-processed photodetectors based on different materials and platforms, compared to their best standard bulk reference counterparts (dashed lines). Only measured specific detectivities are reported in this chart. **b**,**c** | Plots of detectivity versus bandwidth (panel **b**) and external quantum efficiency (EQE) versus bandwidth (panel **c**) are shown for colloidal quantum dot (CQD), organic and metal-halide perovskite photodetectors, illustrating the gain–noise–bandwidth compromise. The advent of metal-halide perovskite photodetectors resulted in significant improvements in visible sensitivities, as well as in detectivity–bandwidth and EQE–bandwidth products. Hybrid phototransistors and photo junction field-effect transistors also led to remarkable advances, surpassing the $10^8$ Hz EQE–bandwidth limit. A more detailed version of this figure with references can be found in the Supplementary information S1 (figure). BW, −3dB bandwidth; BLIP, background limited infrared photodetection; CMT, cadmium mercury telluride; MHP, metal-halide perovskite; MIR, mid-infrared; NC, nanocrystal; NIR, near-infrared; OSC, organic semiconductor; PC, photoconductor; PD, photodetector; PT, phototransistor; SWIR, short-wave infrared; UV, ultraviolet; Vis, visible.

actively manipulate the carrier injection from the CQD layer into graphene, which led to significant improvements in time response (bandwidth, BW ≈ 1.5 kHz), injection efficiencies (approaching 100%) and detectivity ($D^*$ ≈ $10^{13}$ Jones)[81].

Great advances can also be attained through materials chemistry. For example, a method has recently been developed that hugely improves the sensitivity of CdTe photoconductors by manipulating the lifetime and transport domains of majority and minority carriers, resulting in detectivities of up to $5 \times 10^{17}$ Jones in the visible–near-infrared region[82].

An open challenge is the implementation of solution-processed sensors with good performance in the mid-infrared region, a spectral range of importance for spectroscopy and aerospace or astronomy imaging applications. Although breakthroughs have been reported both in terms of materials and of devices[83], there is still much room for improvement to match, or surpass, the performance of standard HgCdTe composite photodetectors, which currently show $D^*$ on the order of ~$10^{10}$ Jones at 10 μm. These narrow-bandgap materials could especially benefit from integration into hybrid phototransistor architectures. Intraband photodetection (involving a $1S_e$–$1P_e$ transition between the first two conduction-band states of the quantum dot) was demonstrated in HgSe CQDs[84]. A precise doping of the nanocrystals is required to populate the $1S_e$ state, which gives rise to photosensitization up to 5 μm. This new strategy opens the way to colloidal infrared photodetectors that go beyond classic interband sensitization. If used for aerospace or defence applications, infrared photodetectors will need to fulfil stringent performance requirements under harsh conditions, which will open exciting directions of research for the next decade.

Apart from sensitive photodetection, there is demand for fast photodetection, which is crucial for communication and time-of-flight imaging. The temporal response of solution-processed photodetectors still needs to be improved to match that of their best crystalline semiconductor counterparts, which remain the dominant technology. Although several materials and architectures exhibit sub-millisecond response times (suitable for the national television system committee (NTSC) and phase-alternating line (PAL) frame-rate video standards), the read-out process within CMOS electronic circuits still relies on speeds high enough for a full pixel column to be read within a frame time.

A chart comparing the value of $D^*$ with the −3dB bandwidth of different materials and architectures reveals a high degree of variability for these metrics (FIG. 4b). There is a clear difference in the BW × $D^*$ performance of different materials and an apparent compromise between speed, sensitivity and spectral coverage, because the realization of high-quality materials becomes more challenging for lower bandgaps. Organic and organohalide semiconductors in general exhibit higher BW × $D^*$ products for visible and near-infrared photodetection[57]. In CQDs, quantum funnelling allows $D^*$ of over $10^{13}$ Jones to be achieved with remarkable >1 MHz bandwidths for visible–near-infrared imaging[46]. In the short-wave infrared region, this metric has been maximized in CQD photodiodes with a bandwidth of 5 MHz and $D^*$ ≈ $10^{12}$ Jones[8]. To this point, MHPs represent the most promising route for achieving higher BW × $D^*$ products. Infrared-sensitization could be achieved by combining them with other materials, such as CQDs, in standard or hybrid phototransistor architectures in the attempt to obtain similar or higher values for this metric in the infrared region.

These differences between materials are also evident in the gain–bandwidth product (FIG. 4c). CQD photoconductors exhibit the largest gains, but at the expense of moderate bandwidths. The best reported $G \times$ BW products (above $6 \times 10^6$ Hz) correspond to visible CdS photoconductors with improved carrier mobility[37]. Organic and organohalide perovskites showcase a better performance, and organic photodiodes with BW up to 430 MHz (but gainless) with $G \times$ BW values over $10^8$ Hz were reported[85].

This threshold was not surpassed until the advent of hybrid CQD (~$10^8$ Hz) and perovskite (~$10^7$ Hz) phototransistors[69], which demonstrates the benefit of using hybrid photodetection approaches to break the $G \times$ BW compromise even for lower bandgap materials. More recently, the rapid progress in MHPs materials processing has led to the realization of methyl-ammonium lead bromide single crystals that, implemented in a back-to-back Schottky photodetector architecture, resulted in a $G \times$ BW beyond the $10^8$ Hz threshold[86]. Ultrafast infrared photodetection with moderate quantum efficiencies has recently been reported in nanosized PbSe microstrip photodetectors[87].

From a materials perspective, exciting directions are opened by the use of recently reported material platforms. New hybrid materials such as quantum-dot-in-perovskite solids[88] (which epitaxially incorporate CQDs in a perovskite matrix), 2D and quasi-2D perovskites[89] (which have tunable bandgaps and anisotropic mobilities) or perovskite-based nanocrystals[90] might open the way to unconventional photodetection schemes stemming from their particular material properties, or allow the efficient revisiting of traditional approaches used in crystalline semiconductors, such as avalanche[91] or quantum-well photodetectors[92,93]. The realization of efficient all-solution-processed photodetectors is also an attractive route towards flexible and wearable photodetectors[94].

As an example of where this technology may take us, in the next section we discuss new functionalities enabled by the use of solution-processed materials that allow the realization of single-pixel multispectral narrowband photodetectors.

## Wavelength-selective photodetection

Wavelength-selective photodetection is needed to achieve colour discrimination, which is crucial for many applications such as colour photography, machine vision, gaming and intelligent surveillance. Current image sensors are based on broadband photojunctions integrated with optical filter arrays to attain colour selectivity (FIG. 5a). In standard camera sensors, the use of passive colour filter arrays limits the spatial resolution and causes colour constancy problems under different

illumination conditions. Although passive filters can deliver enough colour discrimination to reconstruct standard colour photographs, they are not ideal for machine vision and object recognition because their spectral response at different colours strongly overlaps.

Stacked image sensors, in which individual layers collect different colours (FIG. 5b), have been implemented based on organic semiconductors[95–98] or CQDs[34]. This approach, which results in increased sensor resolution, requires a careful design to avoid vertical colour-crossover arising from incomplete absorption. The implementation of stacked image sensors into top-surface photodetectors or back-surface-illuminated architectures requires the use of transparent thin-film transistors[97] with a 100% fill factor.

The use of single materials for highly colour-selective imaging is especially attractive for machine vision and convenient for ROIC integration. To this end, narrowband-absorbing organic semiconductors which can potentially deliver the narrowband responses required for machine vision have been explored[3]. However, these devices often use a blend of donor and acceptor molecules (predominantly fullerenes) that contribute to the photocurrent generation and need to be optimized in terms of the spectral shape of light absorption. This optimization has been implemented for the donor[4,99], but not for the acceptor.

A new approach paradoxically uses broadband absorbers to deliver narrowband spectral responses[3,100]. Broadband-absorbing polymer–fullerene systems have been used in optically thick junctions (1.5–3 μm) and delivered narrowband spectral responses in the red and near-infrared regions with full width at half maximum (FWHM) resonance width smaller than 100 nm, $D^*$ exceeding $10^{12}$ Jones and −3dB frequency bandwidth of hundreds of kilohertz[3]. The underlying mechanism, in which only the charges generated in the volume of the active layer are collected, has been termed charge collection narrowing (CCN, FIG. 5c). The idea is based on the fact that the electro-optics of thick junctions (of thickness $d > \mu m$) is substantially different from that of thin photodiodes ($d \approx 100$ nm). Recent studies further support this concept[101]. In particular, it was shown that depending on the electron–hole mobility ratio, the junction can be made electrically thicker by choosing either an inverted or a conventional architecture[102]. For a given bulk heterojunction system, all photons with energy greater than the optical gap are absorbed near the surface of the transparent anode, while those at the optical gap, which have a much lower extinction coefficient, can propagate through the cavity. This results in strong absorption and photogeneration in the volume of the heterojunction (FIG. 5d). Surface-generated carriers must travel back to the cathode, resulting in very slow extraction[100]. This gives rise to space charge accumulation near the anode. Conversely, carriers generated within the volume experience a more balanced electron and hole transport and can be more easily extracted.

CCN was proposed as a material-agnostic approach[3], and its usage has now been expanded to MHP films, single crystals and quantum dots[64,103,104]. Red–green–blue narrowband photodiodes were realized[64] by introducing an organic molecular dopant into lead iodide and lead perovskites with different halide ratios. The organic additive reduces the crystallite size and suppresses the mobility, making the junction effectively thicker for charge extraction; simultaneously, it also adjusts the absorption spectrum to the desired shape for CCN (FIG. 5e). Following recent developments in the growth of lead halide perovskite single crystals, ultra-narrowband-response CCN photodiodes (FWHM <20 nm) were developed[104]. As a result of the low energetic disorder of these single crystals, the onset of absorption is sharp, and thus very narrow responses of <20 nm can be achieved (FIG. 5f). CCN has also been achieved in high-gain nanocomposites; for example, spectral narrowing and large gain were simultaneously realized in P3HT:PCBM:CdTe nanocomposites[105].

In summary, colour selectivity through CCN opens the way for efficient sensing suitable for machine vision applications. Whereas the use of single-crystal MHPs is not appealing for consumer optoelectronics, because it requires millimetre-thick slabs that are not compatible with ultrathin compact sensors, the implementation of CCN based on BHJ or molecular-dopant-modified perovskites is compatible with CMOS electronics top-surface photodetection architectures, ultimately allowing for multispectral sensors that combine different functionalities.

Figure 5 | **Colour selectivity and charge collection narrowing. a** | A schematic representation of a standard colour filter array on top of a top-surface photodetector is shown. The ultrathin nature of the photoactive film minimizes colour crossover, but the presence of the colour filter increases the final sensor thickness. **b** | Stacked photodetectors allow for improved resolution. Their implementation ultimately requires the use of transparent thin-film transistors (TFTs). In this approach, vertical crossover needs to be carefully considered. **c** | Charge collection narrowing (CCN) can provide an ultra-narrowband photoresponse based on broadband absorbers. **d** | Polymer–fullerene systems have been used in organic thick-junction photodiodes. Within this approach, surface-generated electrons (corresponding to high absorption coefficient) must travel back to the cathode, resulting in very slow extraction, whereas photons corresponding to small absorption coefficients propagate through the material leading to low finesse cavity interference and resulting in strong absorption and photogeneration in the volume of the device. The external quantum efficiency (EQE) displays a narrowband behaviour that can be tuned from the visible to the near-infrared (bottom). **e** | The same concept can be applied to metal-halide perovskite thick-junction photodiodes, in which the presence of organic additive reduces the crystallite size, lowering the mobility and increasing the junction's effective electrical thickness, and adjusting the absorption spectrum to the desired shape for CCN. **f** | Millimetre-thick single-crystal organohalide perovskites can be used for ultranarrow CCN as a result of their low energetic disorder. This approach has led to the realization of ultranarrow EQE photodetectors[104]. ROIC, read-out integrated circuitry. Panel **f** is adapted with permission from REF. 104, Macmillan Publishers Limited.

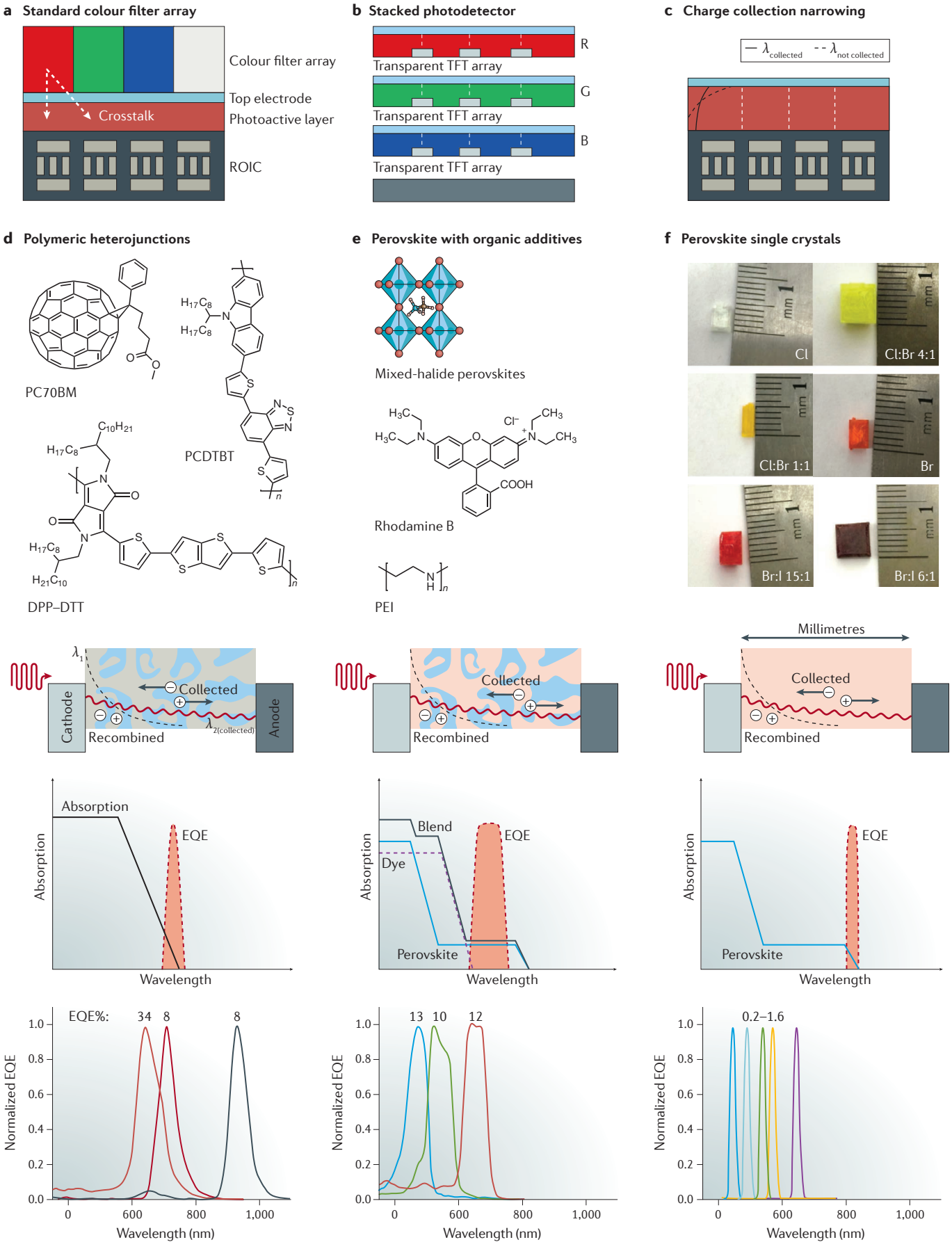

## Conclusion

Photodetection based on solution-processed semiconductors has progressed tremendously during the past decade, owing to advances in material science and device engineering. This has led to sensors that combine desirable manufacturing advantages and state-of-the-art performance metrics for a range of applications. The emergence of materials such as organohalide perovskites offers further transformative improvements that stem from their exceptional optoelectronic properties. New hybrid phototransistor architectures that overcome the classic photodetection limits have been introduced. Filterless, colour selective, multispectral narrowband photodetection is now a real possibility and will allow high-purity, compact image sensors with high spatial resolution and pure colour replication. As laboratory ideas mature into technological realities, exciting times are ahead for photodetection.


1. Suzuki, T. Challenges of image-sensor development. *IEEE Int. Solid-State Circuits Conf. (ISSCC)* 27–30 (2010).
2. Lee, K.-H. *et al.* Dynamic characterization of green-sensitive organic photodetectors using nonfullerene small molecules: frequency response based on the molecular structure. *J. Phys. Chem. C* **118**, 13424–13431 (2014).
3. Armin, A., Jansen-van Vuuren, R. D., Kopidakis, N., Burn, P. L. & Meredith, P. Narrowband light detection via internal quantum efficiency manipulation of organic photodiodes. *Nat. Commun.* **6**, 6343 (2015).
4. Lyons, D. M. *et al.* Narrow band green organic photodiodes for imaging. *Org. Electron.* **15**, 2903–2911 (2014).
5. Gong, X. *et al.* High-detectivity polymer photodetectors with spectral response from 300 nm to 1450 nm. *Science* **325**, 1665–1667 (2009).
6. Armin, A. *et al.* Thick junction broadband organic photodiodes. *Laser Photonics Rev.* **8**, 924–932 (2014).
7. Konstantatos, G. *et al.* Ultrasensitive solution-cast quantum dot photodetectors. *Nature* **442**, 180–183 (2006).
8. Clifford, J. P. *et al.* Fast, sensitive and spectrally tuneable colloidal-quantum-dot photodetectors. *Nat. Nanotechnol.* **4**, 40–44 (2009).
9. Saran, R. & Curry, R. J. Lead sulphide nanocrystal photodetector technologies. *Nat. Photonics* **10**, 81–92 (2016).
10. Mohd Yusoff, A. R. Bin & Nazeeruddin, M. K. Organohalide lead perovskites for photovoltaic applications. *J. Phys. Chem. Lett.* **7**, 851–866 (2016).
11. Brenner, T. M., Egger, D. A., Kronik, L., Hodes, G. & Cahen, D. Hybrid organic–inorganic perovskites: low-cost semiconductors with intriguing charge-transport properties. *Nat. Rev. Mater.* **1**, 15007 (2016).
12. Sze, S. M. *Physics of Semiconductor Devices* (Wiley, 1981).
13. McNeill, R., Siudak, R., Wardlaw, J. & Weiss, D. Electronic conduction in polymers. I. The chemical structure of polypyrrole. *Aust. J. Chem.* **16**, 1056–1075 (1963).
14. Tang, C. W. Photovoltaic effects of metal–chlorophyll-a–metal sandwich cells. *J. Chem. Phys.* **62**, 2139 (1975).
15. Koezuka, H., Tsumura, A. & Ando, T. Field-effect transistor with polythiophene thin film. *Synth. Met.* **18**, 699–704 (1987).
16. Baeg, K.-J., Binda, M., Natali, D., Caironi, M. & Noh, Y.-Y. Organic light detectors: photodiodes and phototransistors. *Adv. Mater.* **25**, 4267–4295 (2013).
17. Harrison, M. G., Grüner, J. & Spencer, G. C. W. Analysis of the photocurrent action spectra of MEH-PPV polymer photodiodes. *Phys. Rev. B* **55**, 7831–7849 (1997).
18. Armin, A. *et al.* Spectral dependence of the internal quantum efficiency of organic solar cells: effect of charge generation pathways. *J. Am. Chem. Soc.* **136**, 11465–11472 (2014).
19. Fang, Y., Guo, F., Xiao, Z. & Huang, J. Large gain, low noise nanocomposite ultraviolet photodetectors with a linear dynamic range of 120 dB. *Adv. Opt. Mater.* **2**, 348–353 (2014).
20. Li, L., Huang, Y., Peng, J., Cao, Y. & Peng, X. Highly responsive organic near-infrared photodetectors based on a porphyrin small molecule. *J. Mater. Chem. C* **2**, 1372 (2014).
21. Yao, Y. *et al.* Plastic near-infrared photodetectors utilizing low band gap polymer. *Adv. Mater.* **19**, 3979–3983 (2007).
22. Pierre, A., Deckman, I., Lechêne, P. B. & Arias, A. C. High detectivity all-printed organic photodiodes. *Adv. Mater.* **27**, 6411–6417 (2015).
23. You, J. *et al.* A polymer tandem solar cell with 10.6% power conversion efficiency. *Nat. Commun.* **4**, 1446 (2013).
24. Coffin, R. C., Peet, J., Rogers, J. & Bazan, G. C. Streamlined microwave-assisted preparation of narrow-bandgap conjugated polymers for high-performance bulk heterojunction solar cells. *Nat. Chem.* **1**, 657–661 (2009).
25. Armin, A. *et al.* Quantum efficiency of organic solar cells: electro-optical cavity considerations. *ACS Photonics* **1**, 173–181 (2014).
26. Lupton, J. M. *et al.* Organic microcavity photodiodes. *Adv. Mater.* **15**, 1471–1474 (2003).
27. Qi, J. *et al.* Panchromatic small molecules for UV–Vis–NIR photodetectors with high detectivity. *J. Mater. Chem. C* **2**, 2431 (2014).
28. Rauch, T. *et al.* Near-infrared imaging with quantum-dot-sensitized organic photodiodes. *Nat. Photonics* **3**, 332–336 (2009).
29. Guo, F. *et al.* A nanocomposite ultraviolet photodetector based on interfacial trap-controlled charge injection. *Nat. Nanotechnol.* **7**, 798–802 (2012).
30. Dong, R. *et al.* An ultraviolet-to-NIR broad spectral nanocomposite photodetector with gain. *Adv. Opt. Mater.* **2**, 549–554 (2014).
31. Greenham, N. C., Peng, X. & Alivisatos, A. P. Charge separation and transport in conjugated-polymer/semiconductor-nanocrystal composites studied by photoluminescence quenching and photoconductivity. *Phys. Rev. B* **54**, 17628–17637 (1996).
32. Oertel, D. C., Bawendi, M. G., Arango, A. C. & Bulović, V. Photodetectors based on treated CdSe quantum-dot films. *Appl. Phys. Lett.* **87**, 213505 (2005).
33. McDonald, S. a *et al.* Solution-processed PbS quantum dot infrared photodetectors and photovoltaics. *Nat. Mater.* **4**, 138–142 (2005).
34. Konstantatos, G., Clifford, J., Levina, L. & Sargent, E. H. Sensitive solution-processed visible-wavelength photodetectors. *Nat. Photonics* **1**, 531–534 (2007).
35. Konstantatos, G. & Sargent, E. H. PbS colloidal quantum dot photoconductive photodetectors: transport, traps, and gain. *Appl. Phys. Lett.* **91**, 173505 (2007).
36. Konstantatos, G., Levina, L., Fischer, A. & Sargent, E. H. Engineering the temporal response of photoconductive photodetectors via selective introduction of surface trap states. *Nano Lett.* **8**, 1446–1450 (2008).
37. Lee, J.-S., Kovalenko, M. V., Huang, J., Chung, D. S. & Talapin, D. V. Band-like transport, high electron mobility and high photoconductivity in all-inorganic nanocrystal arrays. *Nat. Nanotechnol.* **6**, 348–352 (2011).
38. Kim, S. J., Kim, W. J., Sahoo, Y., Cartwright, A. N. & Prasad, P. N. Multiple exciton generation and electrical extraction from a PbSe quantum dot photoconductor. *Appl. Phys. Lett.* **92**, 31107 (2008).
39. Sukhovatkin, V., Hinds, S., Brzozowski, L. & Sargent, E. H. Colloidal quantum-dot photodetectors exploiting multiexciton generation. *Science* **324**, 1542–1544 (2009).
40. Ka, I. *et al.* Multiple exciton generation induced enhancement of the photoresponse of pulsed-laser-ablation synthesized single-wall-carbon-nanotube/PbS-quantum-dots nanohybrids. *Sci. Rep.* **6**, 20083 (2016).
41. Gao, J., Fidler, A. F. & Klimov, V. I. Carrier multiplication detected through transient photocurrent in device-grade films of lead selenide quantum dots. *Nat. Commun.* **6**, 8185 (2015).
42. Nair, G., Geyer, S. M., Chang, L.-Y. & Bawendi, M. G. Carrier multiplication yields in PbS and PbSe nanocrystals measured by transient photoluminescence. *Phys. Rev. B* **78**, 125325 (2008).
43. Clifford, J. P., Johnston, K. W., Levina, L. & Sargent, E. H. Schottky barriers to colloidal quantum dot films. *Appl. Phys. Lett.* **91**, 253117 (2007).
44. Pal, B. N. *et al.* High-sensitivity p–n junction photodiodes based on PbS nanocrystal quantum dots. *Adv. Funct. Mater.* **22**, 1741–1748 (2012).
45. Szendrei, K. *et al.* Solution-processable near-IR photodetectors based on electron transfer from PbS nanocrystals to fullerene derivatives. *Adv. Mater.* **21**, 683–687 (2009).
46. Kim, J. Y. *et al.* Single-step fabrication of quantum funnels via centrifugal colloidal casting of nanoparticle films. *Nat. Commun.* **6**, 7772 (2015).
47. Pelayo García de Arquer, F., Beck, F. J., Bernechea, M. & Konstantatos, G. Plasmonic light trapping leads to responsivity increase in colloidal quantum dot photodetectors. *Appl. Phys. Lett.* **100**, 43101 (2012).
48. Beck, F. J., Stavrinadis, A., Diedenhofen, S. L., Lasanta, T. & Konstantatos, G. Surface plasmon polariton couplers for light trapping in thin-film absorbers and their application to colloidal quantum dot optoelectronics. *ACS Photonics* **1**, 1197–1205 (2014).
49. Diedenhofen, S. L., Kufer, D., Lasanta, T. & Konstantatos, G. Integrated colloidal quantum dot photodetectors with color-tunable plasmonic nanofocusing lenses. *Light Sci. Appl.* **4**, e234 (2015).
50. Beck, F. J., García de Arquer, F. P., Bernechea, M. & Konstantatos, G. Electrical effects of metal nanoparticles embedded in ultra-thin colloidal quantum dot films. *Appl. Phys. Lett.* **101**, 41103 (2012).
51. García de Arquer, F. P., Lasanta, T., Bernechea, M. & Konstantatos, G. Tailoring the electronic properties of colloidal quantum dots in metal-semiconductor nanocomposites for high performance photodetectors. *Small* **11**, 2636–2641 (2015).
52. Lin, Q., Armin, A., Nagiri, R. C. R., Burn, P. L. & Meredith, P. Electro-optics of perovskite solar cells. *Nat. Photonics* **9**, 106–112 (2014).
53. Kojima, A., Teshima, K., Shirai, Y. & Miyasaka, T. Organometal halide perovskites as visible-light sensitizers for photovoltaic cells. *J. Am. Chem. Soc.* **131**, 6050–6051 (2009).
54. Lee, M. M., Teuscher, J., Miyasaka, T., Murakami, T. N. & Snaith, H. J. Efficient hybrid solar cells based on meso-superstructured organometal halide perovskites. *Science* **338**, 643–647 (2012).
55. Hu, X. *et al.* High-performance flexible broadband photodetector based on organolead halide perovskite. *Adv. Funct. Mater.* **24**, 7373–7380 (2014).
56. Lin, Q., Armin, A., Lyons, D. M., Burn, P. L. & Meredith, P. Low noise, IR-blind organohalide perovskite photodiodes for visible light detection and imaging. *Adv. Mater.* **27**, 2060–2064 (2015).
57. Dou, L. *et al.* Solution-processed hybrid perovskite photodetectors with high detectivity. *Nat. Commun.* **5**, 5404 (2014).
58. Sutherland, B. R. *et al.* Sensitive, fast, and stable perovskite photodetectors exploiting interface engineering. *ACS Photonics* **2**, 1117–1123 (2015).
59. Fang, Y. & Huang, J. Resolving weak light of sub-picowatt per square centimeter by hybrid perovskite photodetectors enabled by noise reduction. *Adv. Mater.* **27**, 2804–2810 (2015).
60. Liu, M., Johnston, M. B. & Snaith, H. J. Efficient planar heterojunction perovskite solar cells by vapour deposition. *Nature* **501**, 395–398 (2013).

61. Jeon, N. J. *et al.* Solvent engineering for high-performance inorganic–organic hybrid perovskite solar cells. *Nat. Mater.* **13**, 897–903 (2014).
62. Dong, R. *et al.* High-gain and low-driving-voltage photodetectors based on organolead triiodide perovskites. *Adv. Mater.* **27**, 1912–1918 (2015).
63. Liu, C. *et al.* Ultrasensitive solution-processed broadband photodetectors using $CH_3NH_3PbI_3$ perovskite hybrids and PbS quantum dots as light harvesters. *Nanoscale* **7**, 16460–16469 (2015).
64. Lin, Q., Armin, A., Burn, P. L. & Meredith, P. Filterless narrowband visible photodetectors. *Nat. Photonics* **9**, 687–694 (2015).
65. Yakunin, S. *et al.* Detection of X-ray photons by solution-processed lead halide perovskites. *Nat. Photonics* **9**, 444–449 (2015).
66. Wei, H. *et al.* Sensitive X-ray detectors made of methylammonium lead tribromide perovskite single crystals. *Nat. Photonics* **10**, 333–339 (2016).
67. Shah, K. *et al.* Lead iodide X-ray detection systems. *Nucl. Instrum. Methods Phys. Res. A* **380**, 266–270 (1996).
68. Gu, P., Yao, Y., Feng, L., Niu, S. & Dong, H. Recent advances in polymer phototransistors. *Polym. Chem.* **6**, 7933–7944 (2015).
69. Konstantatos, G. *et al.* Hybrid graphene–quantum dot phototransistors with ultrahigh gain. *Nat. Nanotechnol.* **7**, 363–368 (2012).
70. Sun, Z. *et al.* Infrared photodetectors based on CVD-grown graphene and PbS quantum dots with ultrahigh responsivity. *Adv. Mater.* **24**, 5878–5883 (2012).
71. Wang, Y. *et al.* Hybrid graphene–perovskite phototransistors with ultrahigh responsivity and gain. *Adv. Opt. Mater.* **3**, 1389–1396 (2015).
72. Lee, Y. *et al.* High-performance perovskite–graphene hybrid photodetector. *Adv. Mater.* **27**, 41–46 (2015).
73. Li, F. *et al.* Ambipolar solution-processed hybrid perovskite phototransistors. *Nat. Commun.* **6**, 8238 (2015).
74. Kufer, D. *et al.* Hybrid 2D–0D $MoS_2$–PbS quantum dot photodetectors. *Adv. Mater.* **27**, 176–180 (2015).
75. Kufer, D. & Konstantatos, G. Highly sensitive, encapsulated $MoS_2$ photodetector with gate controllable gain and speed. *Nano Lett.* **15**, 7307–7313 (2015).
76. Kufer, D. & Konstantatos, G. Photo-FETs: phototransistors enabled by 2D and 0D nanomaterials. *ACS Photonics* **3**, 2197–2210 (2016).
77. Yuan, Y. *et al.* Solution-processed nanoparticle super-float-gated organic field-effect transistor as un-cooled ultraviolet and infrared photon counter. *Sci. Rep.* **3**, 2707 (2013).
78. Adinolfi, V. *et al.* Photojunction field-effect transistor based on a colloidal quantum dot absorber channel layer. *ACS Nano* **9**, 356–362 (2015).
79. Masala, S. *et al.* The silicon:colloidal quantum dot heterojunction. *Adv. Mater.* **27**, 7445–7450 (2015).
80. Kufer, D., Lasanta, T., Bernechea, M., Koppens, F. H. L. & Konstantatos, G. Interface engineering in hybrid quantum dot–2D phototransistors. *ACS Photonics* **3**, 1324–1330 (2016).
81. Nikitskiy, I. *et al.* Integrating an electrically active colloidal quantum dot photodiode with a graphene phototransistor. *Nat. Commun.* **7**, 11954 (2016).
82. Zhang, Y. *et al.* Ultrasensitive photodetectors exploiting electrostatic trapping and percolation transport. *Nat. Commun.* **7**, 11924 (2016).
83. Keuleyan, S., Lhuillier, E., Brajuskovic, V. & Guyot-Sionnest, P. Mid-infrared HgTe colloidal quantum dot photodetectors. *Nat. Photonics* **5**, 489–493 (2011).
84. Deng, Z., Jeong, K. S. & Guyot-Sionnest, P. Colloidal quantum dots intraband photodetectors. *ACS Nano* **8**, 11707–11714 (2014).
85. Peumans, P., Bulović, V. & Forrest, S. R. Efficient, high-bandwidth organic multilayer photodetectors. *Appl. Phys. Lett.* **76**, 3855 (2000).
86. Saidaminov, M. I. *et al.* Planar-integrated single-crystalline perovskite photodetectors. *Nat. Commun.* **6**, 8724 (2015).
87. Gao, J., Nguyen, S. C., Bronstein, N. D. & Alivisatos, A. P. Solution-processed, high-speed, and high-quantum-efficiency quantum dot infrared photodetectors. *ACS Photonics* **3**, 1217–1222 (2016).
88. Ning, Z. *et al.* Quantum-dot-in-perovskite solids. *Nature* **523**, 324–328 (2015).
89. Saparov, B. & Mitzi, D. B. Organic–inorganic perovskites: structural versatility for functional materials design. *Chem. Rev.* **116**, 4558–4596 (2016).
90. Ramasamy, P. *et al.* All-inorganic cesium lead halide perovskite nanocrystals for photodetector applications. *Chem. Commun. (Camb.)* **52**, 2067–2070 (2016).
91. Hayden, O., Agarwal, R. & Lieber, C. M. Nanoscale avalanche photodiodes for highly sensitive and spatially resolved photon detection. *Nat. Mater.* **5**, 352–356 (2006).
92. Martyniuk, P. & Rogalski, A. Quantum-dot infrared photodetectors: status and outlook. *Prog. Quantum Electron.* **32**, 89–120 (2008).
93. Rogalski, A. *Infrared Detectors* (CRC, 2010).
94. Choi, J.-H. *et al.* Exploiting the colloidal nanocrystal library to construct electronic devices. *Science* **352**, 205–208 (2016).
95. Aihara, S. *et al.* Stacked image sensor with green- and red-sensitive organic photoconductive films applying zinc oxide thin-film transistors to a signal readout circuit. *IEEE Trans. Electron. Devices* **56**, 2570–2576 (2009).
96. Antognazza, M. R., Scherf, U., Monti, P. & Lanzani, G. Organic-based tristimuli colorimeter. *Appl. Phys. Lett.* **90**, 163509 (2007).
97. Seo, H. *et al.* A 128 × 96 pixel stack-type color image sensor: stack of individual blue-, green-, and red-sensitive organic photoconductive films integrated with a ZnO thin film transistor readout circuit. *Jpn J. Appl. Phys.* **50**, 24103 (2011).
98. Lim, S.-J. *et al.* Organic-on-silicon complementary metal-oxide-semiconductor colour image sensors. *Sci. Rep.* **5**, 7708 (2015).
99. Jansen-van Vuuren, R. D., Pivrikas, A., Pandey, A. K. & Burn, P. L. Colour selective organic photodetectors utilizing ketocyanine-cored dendrimers. *J. Mater. Chem. C* **1**, 3532 (2013).
100. Johnston, M. B. Optoelectronics: colour-selective photodiodes. *Nat. Photonics* **9**, 634–636 (2015).
101. Tait, J. G. *et al.* Interfacial depletion regions: beyond the space charge limit in thick bulk heterojunctions. *ACS Appl. Mater. Interfaces* **8**, 2211–2219 (2016).
102. Armin, A. *et al.* Electro-optics of conventional and inverted thick junction organic solar cells. *ACS Photonics* **2**, 1745–1754 (2015).
103. Qiao, K. *et al.* Spectra-selective PbS quantum dot infrared photodetectors. *Nanoscale* **8**, 7137–7143 (2016).
104. Fang, Y., Dong, Q., Shao, Y., Yuan, Y. & Huang, J. Highly narrowband perovskite single-crystal photodetectors enabled by surface-charge recombination. *Nat. Photonics* **9**, 679–686 (2015).
105. Shen, L., Fang, Y., Wei, H., Yuan, Y. & Huang, J. A. Highly sensitive narrowband nanocomposite photodetector with gain. *Adv. Mater.* **28**, 2043–2048 (2016).
106. Gong, X. *et al.* Semiconducting polymer photodetectors with electron and hole blocking layers: high detectivity in the near-infrared. *Sensors (Basel)* **10**, 6488–6496 (2010).
107. Liu, X., Wang, H., Yang, T., Zhang, W. & Gong, X. Solution-processed ultrasensitive polymer photodetectors with high external quantum efficiency and detectivity. *ACS Appl. Mater. Interfaces* **4**, 3701–3705 (2012).
108. Hu, X. *et al.* High-detectivity inverted near-infrared polymer photodetectors using cross-linkable conjugated polyfluorene as an electron extraction layer. *J. Mater. Chem. C* **2**, 9592–9598 (2014).
109. Liu, C. *et al.* Ultrasensitive solution-processed perovskite hybrid photodetectors. *J. Mater. Chem. C* **3**, 6600–6606 (2015).
110. Liu, H., Lhuillier, E. & Guyot-Sionnest, P. 1/*f* noise in semiconductor and metal nanocrystal solids. *J. Appl. Phys.* **115**, 154309 (2014).
111. Solis-Ibarra, D., Smith, I. C. & Karunadasa, H. I. Post-synthetic halide conversion and selective halogen capture in hybrid perovskites. *Chem. Sci.* **6**, 4054–4059 (2015).
112. Filip, M. R., Eperon, G. E., Snaith, H. J. & Giustino, F. Steric engineering of metal-halide perovskites with tunable optical band gaps. *Nat. Commun.* **5**, 5757 (2014).
113. Lin, Q., Stoltzfus, D. M., Armin, A., Burn, P. L. & Meredith, P. An hydrophilic anode interlayer for solution processed organohalide perovskite solar cells. *Adv. Mater. Interfaces* **3**, 1500420 (2016).
114. Yu, G., Wang, J., McElvain, J. & Heeger, A. J. Large-area, full-color image sensors made with semiconducting polymers. *Adv. Mater.* **10**, 1431–1434 (1998).
115. Hamilton, M. C., Martin, S. & Kanicki, J. Thin-film organic polymer phototransistors. *IEEE Trans. Electron. Devices* **51**, 877–885 (2004).
116. Agostinelli, T. *et al.* A polymer/fullerene based photodetector with extremely low dark current for X-ray medical imaging applications. *Appl. Phys. Lett.* **93**, 203305 (2008).
117. Guo, F., Xiao, Z. & Huang, J. Fullerene photodetectors with a linear dynamic range of 90 dB enabled by a cross-linkable buffer layer. *Adv. Opt. Mater.* **1**, 289–294 (2013).
118. Zhang, H. *et al.* Transparent organic photodetector using a near-infrared absorbing cyanine dye. *Sci. Rep.* **5**, 9439 (2015).



**Acknowledgements**

P.M. is an Australian Research Council Discovery Outstanding Research Award Fellow, and a Ser Cymru Research Chair funded under the Ser Cymru II Program by the Welsh Assembly Government and the Welsh European Funding Office. A.A. and P.M. acknowledge funding from the Australian Research Council through the Discovery Program and the Australian Centre for Advanced Photovoltaics (Australian Renewable Energy Agency). This work was supported by the Ontario Research Fund: Research Excellence Program, the Natural Sciences and Engineering Research Council (NSERC) of Canada, and the Connaught Global Challenges Program of the University of Toronto.


**Competing interests statement**

The authors declare no competing interests.

**FURTHER INFORMATION**

**InVisage:** http://www.invisage.com/
**OmniVision:** http://www.ovt.com/

**SUPPLEMENTARY INFORMATION**

**See online article:** S1 (figure)

**ALL LINKS ARE ACTIVE IN THE PDF**